JOURNAL OF OPTOELECTRONICS AND ADVANCED MATERIALS Vol. 10, No. 1, January 2008, p. 91 - 97

Computer simulation of micro- and nano- structures at electron and ion lithography

K. VUTOVA*, G. MLADENOV
Institute of Electronics, Bulgarian Academy of Sciences, 72 Tzarigragsko shosse, 1784 Sofia, Bulgaria

In this paper a review concerning the main steps of a complete mathematical model for the simulation of the exposure and development process in electron and ion beam lithography is presented. Our own Monte Carlo simulation tools for electron and ion beam lithographies are applied to the calculation of the energy deposition and the resist-developed profiles of sub-quarter-micron patterns. An example of the pattern deformation due to proximity effects and application of the latent image calculation for the proximity effects correction is also shown. The presented results and comparisons show that the models are adequate and have a very good potential for application in the case of multilayer sub-quarter-micron patterns.

(Received September 25, 2007; accepted January 10, 2008)

Keywords: Electron beam lithography, Ion beam lithography, Computer simulation, Nano-patterning

1. Introduction

Increasing the electronic circuit density is a major trend in microelectronics. Lithography is the key technology for the fabrication of very large integrated circuits with smaller device sizes. Today conventional optical lithography is approaching its fundamental physical limits. Electron and ion lithographies are among various candidates capable of sub-150 nm resolution for the new generation of lithographic techniques. Due to the reasons mentioned above, electron beam lithography (EBL) [1-3] and, recently, ion beam lithography (IBL) [4-6] are currently subject to comprehensive research study. A detailed knowledge of the resist exposure and the development processes, with a view to their optimization, is one of the major problems in this study. Only correct selection of the exposure and development conditions can ensure the necessary higher resolution and the desired developed resist profiles.

In this paper some peculiarities of these methods for nano-structuring through the features of the algorithms used in the computer simulation are discussed. Comparisons between EBL and IBL results obtained by simulation are also presented. Results concerning a correction procedure for EBL are shown.

2. Exposure modeling

2.1. Deposited energy in the case of electron beam lithography simulation

In many simulation tools the scattering in the resist of an electron, incident on one point of the resist film surface, is calculated by the Monte Carlo (MC) method. Random numbers are used for the scattering atom type, choice of the azimuthal scattering angle and estimation of the actual value from a probability function. The scattering angle of the penetrating electron is calculated using the differential scattering cross-section for the penetrating electron (for elastic collisions with target atoms taking into account also the inelastic scattering probability for collisions with an electron of the atom) and assuming a Rutherford shielding potential presenting the scattering atom. The energy loss, as a result of inelastic scattering, is calculated using Bethe stopping power theory. The electron trajectory is assumed as a zigzag path, consisting of straight-line segments with definite lengths (Fig. 1a). The calculation continues until the previously chosen cut-off conditions are not reached. The distance that an electron can travel without changing direction is estimated as the value of the electron free path. The energy loss value is calculated and is written as a matrix (2D array) element, presenting the space position of this quantum absorbed energy in the irradiating resist volume. The trajectory and energy losses on each free path of the penetrating electron are calculated and distributed in this matrix in the respective space positions. These discrete data (array) present the spatial distribution of the energy absorbed in the resist due to a single incident electron. Usually, after this step the exposure energy deposition function (EDF) in the resist film due to a point beam is calculated. The pixel (spot) energy deposition function (SEDF) in the irradiated resist is calculated by convolution of the EDF and the intensity distribution function of the beam electrons in the irradiation spot. Usually, the EDF and SEDF are a sum of Gaussians (sometimes an exponential function is also an additional term in the sum). Hence the energy absorbed at a simple figure (a line, a rectangle) can be calculated using a tabulated Error function that saves computer time. In the next step the irradiated desired image of the produced microstructure is divided into simple figures such as lines or rectangles. The absorbed energy distribution is evaluated by the total result of all simple figures. In MC computer programs one uses about 10 000 trajectories to obtain the SEDF. For an irradiation of a dose of 1μC/cm^2 the number of incident electrons is 62 415 per μm^2. In this way the EDF is calculated in various Monte Carlo programs such as TREM, PRO_BEAM, [7-13] and it can also be obtained by analytical simulation tools such as

SELID [14] for EBL. A two-dimensional data array is the result from a MC calculation of the latent image in the resist layer, i.e. the absorbed energy distribution deposited by electrons in eV/cm^3. The cell size in this array is typically 10-50 nm in the resist depth and in the radial direction from the point of beam incidence.

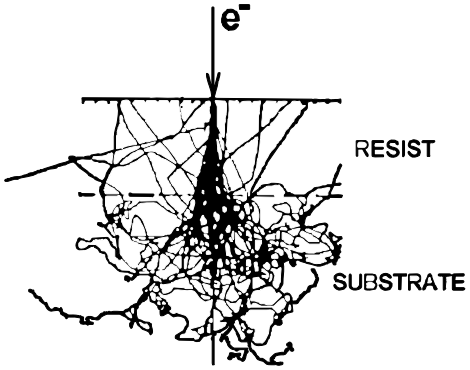

Fig. 1a. Simulated trajectories of 100 electrons in PMMA, the electron energy is 30 keV.

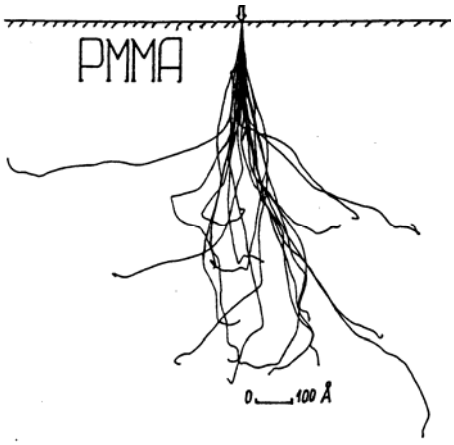

Fig. 1b. 20 simulated trajectories in the case of 6 keV He ions in PMMA.

Due to large lateral scattering of the penetrating electrons, the exposure of many image segments effects the total deposited energy in a specific resist point. This effect, known as a proximity effect, requires high accuracy evaluation of the EDF at large radial distances i.e. far away from the point of incidence. Increasing the trajectory numbers slowly improves the statistics in this region. A Monte Carlo methodology and a corresponding computer program are developed for transformation of the numerical data array, representing the absorbed energy space distribution when exposing one point from the resist surface, into the form of analytical functions [15]. In this way the problem concerning the insufficient statistics of the discrete data for the absorbed energy in the case of large lateral distances is overcome. It is possible to use various cell dimensions at different radial distances: lower values near to the point of beam incidence and higher values far away from this point. When using a Cartesian coordinate system instead of a cylindrical one it is possible to simulate beam incidence inclined to the resist surface [16]. There are procedures for re-calculation of the free path and electron stopping power when a penetrating electron crosses the interfaces in multilayer structures [17].

2.2. Calculation of the deposited energy in the case of ion beam lithography

An accelerated ion changes its own charge state during its movement through the irradiated sample, going from neutralized to the highest charged state depending on the different penetration velocities. Stopping powers and trajectories of the penetrating atom particles in the materials under ion bombardment are quite well understood, due to the progress of ion implantation, ion sputtering and secondary ion mass spectrometry. Computer programs such as MARLOW, TRIM, PIBER, SASAMAL [18-22] were developed between 1970 and 1980. The program structure is the same as for electrons. The major difference is that the energy transfer is executed by two types of losses: nuclear stopping power, due to penetrating particle collisions with the sample atoms and electronic stopping power, due to penetrating projectile collisions with the electrons in the bombarded material.

The first applications of these programs have been for polymethyl methacrylate (PMMA) [21-23] to evaluate the ranges and energy losses. The values of projected and lateral ranges as well as the mean electronic and nuclear stopping powers have been calculated for various penetrating particles at different energies. The displaced secondary atoms in cascades are taken into account. These investigations and results are well known [13,15,23-26].

By such calculations one can see that the scattering and lateral dispersion of the penetrating particles through a resist are small for the ions, which are three orders of magnitude heavier than the electrons. Therefore the proximity effects that are the major problem in the EBL are minimal in the IBL.

There have been many papers in which differences in the resist modification mechanisms during the exposure of polymer resists with electrons and ions have been discussed [4,5,27-35]. In the case of ion irradiation of particular importance was the role of the two types of energy absorption and the experimentally observed enhanced sensitivity of resists (for example PMMA) as well as the excellent resolution [13,32-34]. The following results have been also experimentally observed: a drastic change of the resist structure and resistivity, an increase of the resist optical density and a substantial loss (intense erosion) of the polymer during its ion irradiation with higher doses [36-39].

On the basis of results obtained in ref.[32,33] and which have been confirmed or accepted by few tens of authors, it has been assumed that the electronic energy losses are the main energy absorption mechanism in IBL. The nuclear stopping power has an effect on the solubility modification in the case of heavy low-energy ion irradiation [40]. A new discussion was started in ref.[41]

where considerable disagreement was expressed about the role of electronic losses. It concerns the interpretation of the scission and cross-linking mechanisms, which control the solubility modification of the ion irradiated PMMA. In ref.[41] Lee concluded that the electronic stopping power is more responsible for cross-linking of PMMA while the nuclear losses are more responsible for scission, although both processes can cause cross linking as well as scission. This conclusion is contrary to the positive images usually obtained after exposure of PMMA (the molecular chains' scission results in an increased solubility). The formation of an insoluble compound after higher ion irradiation doses has been interpreted by Lee [41] as the result of forming a cross-linked polymer. He has neglected the results presented in ref.[36,37,39], especially those concerning the drastic compositional changes of PMMA at higher doses [36,39] by losing O and H atoms (i.e. the resist compound does not remain a polymer at these exposure doses).

3. Modeling of resist development

The goal of the computer simulation of the processes in EBL and IBL is the resist profile prediction of developed patterns after exposure of samples, covered by a sensitive polymer resist layer, which is sensitive to irradiation by accelerated particles. During the exposure process the resist material modifies the local solubility rate. The development of an image is a surface etching phenomenon. A resist profile, due to a changed resist thickness up to full opening of irradiated or non-irradiated areas (respectively, in the case of positive tone or negative tone resists) is created as a result of the development process. The type of radiation is not important when applying the simulation models to the development process for a known distribution of the local solubility rate in the resist layer (i.e. for a given latent image described in the solubility rate terms). Therefore known computer simulation modules for optical lithography such as DEPICT, FAIME, METROPOLE, PROLITH, SAMPLE, SOLID, OPTOLIT [27,42-45] can be used. More detailed knowledge and/or comparison of predicted results with experimental data are needed to obtain correct simulation because of the distinct sensitivity behaviour for various chemistry compositions. Moreover, there are different models (in the mentioned tools) for converting the deposited energy distributions into the solubility rate distributions that can be used to obtain reasonable results. Usually, integrated circuit manufacturers, who use specific simulation tools and resists, keep the fitting parameters and approximations used strictly confidential.

There are a number of simulation models that use cells or straight-line segments presenting the developer-resist interface as a function of the developing time. In our model each evolving point from the developed contour advances along the normal to the profile with its local solubility rate. There is a procedure to increase the contour accuracy by increasing the number of the evolving points in the regions with a significant modified tilt in the pattern. A cubic spline in the 2D case and a bicubic spline in the 3D case are used to describe the developed profiles [13,15].

The conversion of the deposited energy distribution in the resist to the solubility rate distribution in the case of one component polymer resists is based on the radiation modification of the polymer molecular weight. Scission or cross-linking mechanisms are the reason for the changes in the dissolution rate in a chosen resist-developer couple. These local changes of the mean resist molecular weight in the irradiated areas are defined by: the resist initial molecular weight, the exposure dose and the resist radiation yield (efficiency) measured as the number of scissions (cross-linking) per electronvolt (or 100 eV) deposited energy. The dissolution rate of the unexposed areas is an important parameter also. For the next calculation step both dependences: the solubility rate vs. the deposited energy densities or the solubility rate vs. the exposure doses can be used [40,46,47]. In the second dependence the changes of the deposited energy distribution vs. the resist depth are neglected.

In the case of two (or more) component radiation-sensitive resists there is a radiation active component (RAC) characterized with the normalized concentration M. The RAC concentration is uniform in unexposed resist and changes during exposure. During thermal processes (post apply bake and post exposure bake) a decomposition of the RAC and a diffusion of the radiative reaction products can occur. Resist development behavior is a function of M and the coordinates. For chemically amplified resists (CARs) the radiative product (an acid) modifies the base component dissolution rate. The resist solubility rate is an intermediate value between the two limiting rates over the whole exposure range and the value of M varies from 0 to 1, respectively. For CARs the acid modifies the base component solubility rate exponentially. The models for the conversion of the solubility rate through the RAC concentration M and the solubility rate modification by reaction products are described in refs. [48-51].

4. Computer simulation results in EBL and IBL

Using our computer programs for mathematical modeling in EBL and IBL we are able to predict results and to learn more features concerning EBL and IBL in the sub-quarter-micron patterns. Some simulation results in the case of electron beam and ion beam exposure (He^+ ions) and development of a sensitive resist (the exposed resist is PMMA - $C_5H_8O_2$) are presented. Fig. 1a shows an example of the results obtained for a 30 keV point-source e-beam, while Fig.1b presents simulated trajectories for He ions in PMMA. Note that backscattered electrons can emerge at large lateral distances from the axis (Fig. 1a).

In Fig. 2a MC simulation data for the EDF(r) calculated at the resist/silicon substrate interface in the case of EBL are presented. EDF(r) simulation results for 400 nm PMMA on Si in the case of ion beam exposure (He^+ ions with energy 100 keV) are shown in Fig. 2b.

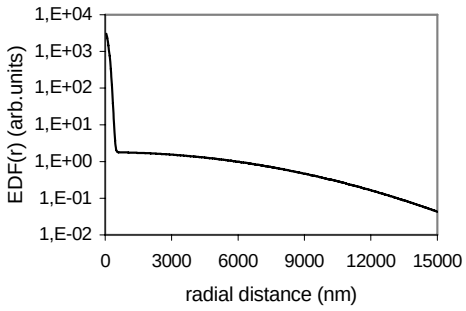

Fig. 2a. EDF(r) simulation at 50 keV e-beam for 400 nm PMMA on Si.

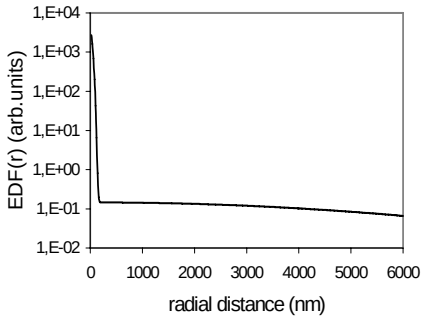

Fig. 2b. Energy deposition at the resist/substrate interface at 100 keV He^+ ion beam.

A 2D simulated resist profile for a line developed in PMMA resist after exposure with 100 keV He^+ ion beam (the image width is 30 nm) is shown in Fig. 3. The beam width is presented by the white band in the black mask on the top of the structure shown in Fig. 3 (the substrate is not shown, the resist layer and the symbolic black mask, added virtually, are indicated). The developed line width is 101 nm at the top of the resist layer. This width is 106nm at the Si substrate while it is 96nm at the narrowest part of the developed line cross-section. This extension of the developed line width is similar to the internal proximity effect. The resist thickness loss during the development process is 7.1%. In Fig. 4 simulation results are provided for three 30nm exposed lines. The development time is 5 min and the doses are: a) 0.25μC/cm^2 for the line in the centre of the figure; b) 0.325μC/cm^2 for the line at x=-1μm; and c) 0.4 μC/cm^2 for the line at x=1μm. One can see the change of the developed profile shapes when varying the exposure dose. The calculated resist thickness loss is 7.3% under these development conditions.

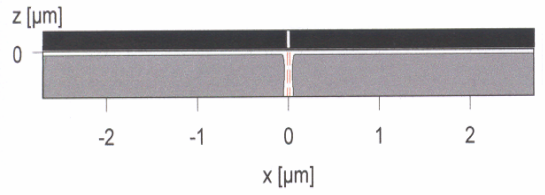

Fig. 3. Simulated resist profiles in the case of 0.03 μm wide isolated long line at a dose of 0.35μm/cm^2, 0.4 μm PMMA/Si, development time - 5 min, 100 keV He ions.

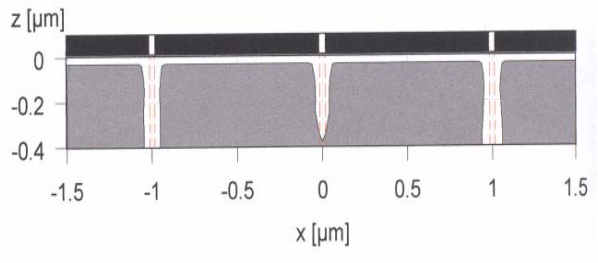

Fig. 4. Simulated resist profiles in the case of three lines for different exposure doses, 100 keV He ions.

Resist profiles of the exposed microstructures (parallel lines and one line between four rectangles) in the case of EBL and IBL are shown in Fig.s 5 and 6. The external proximity effect is not observed in IBL (Figs. 5 and 6a).

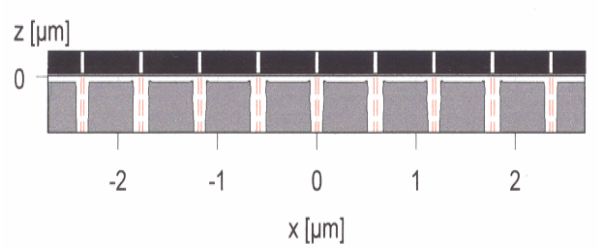

Fig. 5a.Simulated resist profiles for nine 30 nm wide long parallel lines spaced by 560 nm after exposure with 100 keV He^+ ion beam. The resist used is 400 nm thick PMMA on Si.

Fig. 5b. Simulated 3D resist profiles for the layout and the conditions in Fig. 5a (the dose is 350 μC/cm^2, the radiation yield – 0.005, the development time – 5 min).

In Fig. 6b the influence of the proximity effect on the final result of the whole EB lithographic process is presented. After exposure and development of a 30 nm wide line and four 0.8x0.8 μm^2 squares, the developed line width is 410 nm.

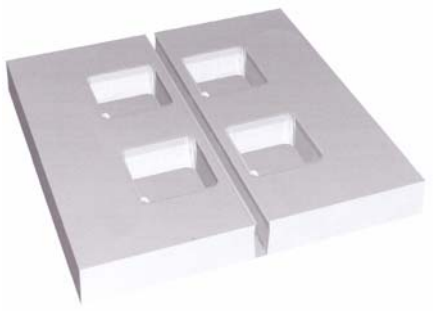

Fig. 6a. Simulated 3D resist profiles for a layout consisting one 0.03 μm wide line and four 0.8 × 0.8 μm² squares after exposure with 100 keV He^+ ion beam.

Fig. 6b. Simulated 3D resist profiles for the layout in fig.6a at 50 keV e-beam. Only the distance between the line and the squares is 635 nm, while it is 185 nm in the case of IBL (Fig.6a).

5. Proximity effects and correction methods in EBL

The proximity effects limit the resolution of EBL. Due to the scattering of electrons in the substrate and resist the penetrating electrons will not only expose resist at the position they are applied, but also in adjacent points, situated up to few microns from the irradiated surface pixel. The result is that the pattern within a low-density region of the exposed image sectors will be underexposed, whereas the pattern in regions of high density will be overexposed. The developed pattern dimensions are determined by the total deposited energy from all the irradiating points in a region defined by the long lateral tail of EDF. The simulations in Fig. 7 show the latent resist image obtained after uncorrected and corrected e-beam exposures in the resist. The deposited exposure energy into the resist can be described as the applied dosage convoluted with the EDF for a simple sector of a desired image (a line, a rectangle).

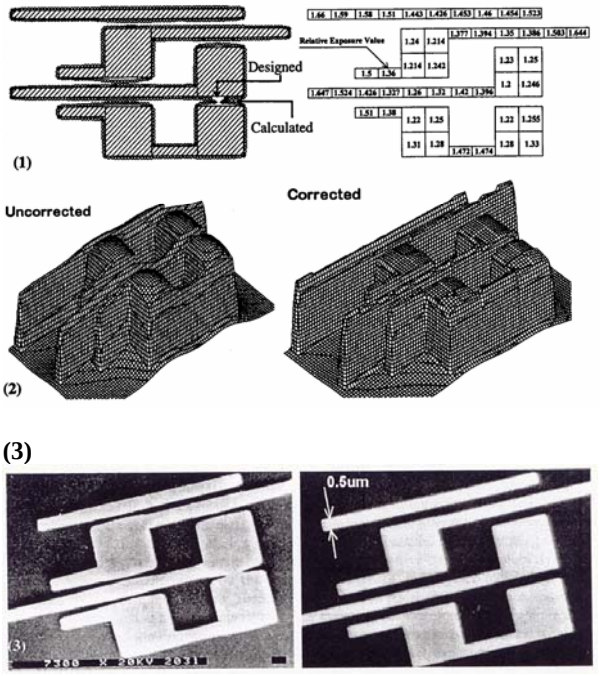

Fig. 7. An example of the pattern deformation due to proximity effects (a) and application of the computational based dose-correction method (b).
(1) (a) simulation of the 2D-pattern contours (b) partitioning and exposure-correction factor;
(2) 3D exposure intensity distribution calculated for (a) uncorrected and (b) corrected exposures;
(3) micrographs of the realised patterns without (a) and with (b) correction.

There are various methods proposed to correct the proximity effects [52-55]. The base approaches are:

(i) *Technology based methods* that use: various beam energies, writing strategies, sophisticated resist and substrate combinations. In many cases, however, technology uses a fixed condition, optimized by different criteria and there is no room to adapt it to the specific problem of proximity effects.

(ii) *Computational proximity effect correction*: the underexposed pattern sectors have to get higher exposure doses and the overexposed parts lower doses. This can be done by changing the time of pixel exposure or the beam current.

The serial variable-shaped lithographic systems allow the exposure process to be corrected with high precision by using a programmable sector-by-sector dosage control and varying the exposure dwell time for individual shapes.

Fig. 7 illustrates a typical example of the proximity affected single rectilinear structure and the same structure after *computational correction*. Lines without larger patterns in the neighbourhood show significantly different line widths than the isolated lines exposed with the same nominal line-width. It often happens, that the narrow gaps between larger patterns become smaller or disappear completely (external proximity effect). In the case of an isolated line the line width changes only (internal

proximity effect) and these changes are significant for wide lines.

For a correction the desired image is partitioned to rectangle sectors (Fig.7.(1)) and the relative exposure value, used for the correction, is shown in the sub-shapes [56].

As shown in Fig. 7, the net result of non-corrected exposure is that the written pattern is a blurred version of the desired pattern. In special cases, if the dimensions of the structure details are strongly reduced, features in close proximity may blur together (external proximity effect). Fig. 7 shows a group of single patterns exposed by EBL with minimal line/space of 0.5 μm. It is evident, that this combination of patterns needs a correction to obtain the desired geometry in the given resist. The original patterns were sub-divided and each fragment assigned an optimum exposure dose by the proximity correction algorithm. The goal is to obtain averaged optimal exposure intensity over the whole structure (without local extremes). Thus, at any point, along the edges of any shape on the pattern, a constant energy value, which equals to threshold exposure intensity, will be deposited. From Fig. 7.(3)b it is evident, that this simple proximity correction procedure significantly improved the geometry and feature size accuracy of the fabricated structures.

6. Conclusions

In the current work a short description of the main steps of the simulation models for EBL and IBL and the peculiarities of the developed MC models are described and discussed. Using the simulation tools the effects of: irradiated particles (electrons and ions), exposure doses and dense patterns are discussed in order to extract the necessary values for high resolution patterning. From the obtained results it is seen that the developed models describe adequately the processes in EBL and IBL. The ion lithography should be considered as one of the competitors for further improvement of the integration level of the produced integral circuits. The simulation results are very useful when optimizing particular technological processes for complex layouts in the sub-quarter-micron lithography.

References

[1] A. Katz, S. Woods, R. Dynes, J. Appl. Phys. **87**, 2978 (2000).
[2] F. Herbstritt, T. Kemen, A. Marx, R. Gross, J. Appl. Phys. **91**, 5411 (2002).
[3] P. Larsson, B. Nillson, Z. Ivanov, J. Vac. Sci. Technol. B, **18**, 25 (2000).
[4] J. Melngailis, A. Mondelli, I. Berry, R. Mohondro, J. Vac. Sci. Technol. B, **16**(3), 927 (1998).
[5] I. Berry, J. Vac. Sci. Technol. B, **16**(4), 2444 (1998).
[6] R. Kaesmaier, H. Loschner Microel. Eng. **53**, 37 (2000).
[7] R. Hawrylik, J. Vac. Sci. Technol.,**1**(19), 1-17 (1981).
[8] S. Hasegawa, Y. Iida, T. Hidaka, J. Vac. Sci. Technol. B, **5**(1), 142-145 (1987).
[9] S. Wind, M. Rosenfeld, G. Pepper, W. Moltzen, P. Gerber, J. Vac. Sci. Technol. B, **7**(6), 1507-1512 (1989).
[10] C. Mack Proc. SPIE **3048**, 76-88 (1997).
[11] G. Mladenov, R. Dimitrova, O. Stojanova, K. Jeleva-Vutova, Proc. of the 1st Intern. Conf. on Electron Beam Technol., Varna, BAS Publ.house (1985), 23.
[12] K. Vutova, G. Mladenov, Thin solid films, **200**, 353-362 (1991).
[13] G. Mladenov, K. Vutova, Proceedings of St.-Petersburg Electrotechnical University, issue "Solid State Physics and Electronics", ed. Boris A. Kalinikos, publisher "SPbGETU LETI", St.-Petersburg, Russia, **1**, 133-173 (2002).
[14] I. Raptis, B. Nowotny, N. Glezos, M. Gentili, G. Meneghini, Jpn. J. Appl. Phys. **39**, 635-644 (2000).
[15] K. Vutova, G. Mladenov, Modelling and Simulation in Materials Science and Engineering, **2**, 239-254 (1994).
[16] Y. Gueorguiev, G. Mladenov, D. Ivanov, J. Vac. Sci. Technol. B, **14**, 2462 (1996).
[17] Y. Gueorguiev, G. Mladenov, D. Ivanov, Thin Solid Films, **251**, 67 (1994).
[18] O. Ouen, M. Robinson, J. Nuclear Mater., **76/77**, 370 (1978).
[19] M. Robinson, I. Torrens Phys. Rev. B, **9**, 5008 (1974).
[20] J. Biersack, L. Haggmark, Nucl. Instr. and Meth., **174**, 257 (1980).
[21] I. Adesida, L. Karapiperis Radiat. Effects **61**, 223-233 (1982).
[22] G. Mladenov, Proceedings of the VII International Conference "Ion implantation in semiconductors and other materials", Vilnus-1983, Publisher AN USSR (1985), 230.
[23] G. Mladenov, M. Braun, B. Emmoth, J. Biersack, J. Appl. Physics **58**, 2534 (1985).
[24] K. Vutova, G. Mladenov, Vacuum **62**, 273-278 (2001).
[25] G. Mladenov, K. Vutova, I. Raptis, P. Argitis, I. Rangelow, Microelectronic Engineering, **57-58**, 335-342 (2001).
[26] K. Vutova, G. Mladenov, Thin Solid Films **214**, 144-149 (1992).
[27] A. Neureuter, D. Kyser, C. Ting, IEEE Trans. Electron Dev. **26**, 686 (1979).
[28] S. Kim, Y. Ham, W. Lee, K. Chun, Microelectron. Eng., **42**, 179 (1998).
[29] S. Aya, T. Hifumi, K. Kise, K. Marumoto,. J. Vac. Sci. Technol. B, **20**, 90 (2002).
[30] V. Ivin, M. Silakov, N. Vorotnikova, D. Resnick, K. Nordquist, L. Siragusa, Microelectron. Eng. **57-58**, 355 (2002).
[31] R. Hawryluk, A. Hawryluk, H. Smith J. Appl. Phys. **45**, 2551 (1974).
[32] G. Mladenov, B. Emmoth, Appl. Phys. Letters, **38**, 1000-1002 (1981).
[33] G. Mladenov, B. Emmoth, M. Braun, Vacuum, **34**, 551-553 (1984).

[34] B. MacIver, J. Electrochem. Soc. Sol. St. Sci. Tech. **129**, 827 (1982),.
[35] N. Glezos, I. Raptis, IEEE Trans. CAD, **15**, 92 (1996).
[36] M. Braun, B. Emmoth, G. Mladenov, H. Satherblom, J. Vac. Sci.. Technol. A, **1**, 1383-1387 (1983).
[37] B. Emmoth, G. Mladenov, J. Appl. Physics **54**, 7119-7123 (1983).
[38] T. Venkatesan, S. Forrest, M. Kaplan, C. Murray, P. Schmidt, B. Wilkens, J. Appl. Phys. **54**, 3150-3153 (1983).
[39] F. Namavar, Budnick J. Nucl. Instr. and Methods in Phys. Res. B1, **5**, 285-287 (1986).
[40] K. Vutova, G. Mladenov, Microelectronic Engineering, **57-58**, 349-353 (2001).
[41] E. Lee, Nucl. Instr. and Meth. in Phys. Res. B1, **51**, 29-41 (1999).
[42] D. Bernard, H. Urbach J. Opt. Soc. Am. A, **8**, 123 (1991).
[43] C. Yuan, A. Strojwas, IEEE Trans. Semicond. Manufact., **4**, 99 (1991).
[44] C. Mack, Proc. SPIE Opt. Microlithography IV, **538**, 207 (1985).
[45] W. Henke, D. Mewes, M. Weib, G. Czech, Schiebl-Hoyler. Microelectr. Eng. **14**, 283 (1991).
[46] M. Komuro, N. Atoda, H. Kawakatsu, J. Electrochem. Soc. **126**, 483 (1979).
[47] J. Greeneich, Ph.D. Dissertation, University of California at Berkeley, (1973).
[48] R. Ferguson, J. Hutchingson, C. Spence, A. Neureuther, J. Vac. Sci. Technol. B, **8**(6), 1423 (1990).
[49] H. Fukuda, S. Okazaki, J. Electrochem. Soc., **137**(2), 675(1990).
[50] N. Tam, H. Liu, C. Spason, A. Neureuther, J. Vac. Sci. Technol. B, **9**(19), 3362 (1991).
[51] M. Weib, H. Binder, R. Schwalm, Microelectronic Engineering, **27**, 405 (1995).
[52] M. Parikh, IBM J. Res. Develop. **24**, 438 (1980).
[53] Y. Pati, A. Teolis, D. Park, R. Bass, K. Rhee, B. Bradie, M. Peckerar, J. Vac. Sci. Technol. B, **8**(6), 1882-1888 (1990).
[54] T. Abe, S. Yamasaki, T. Yamaguchi, R. Yoshikawa, T. Takigawa, Jpn. J. Appl. Phys. **30**(11), 2965-2969 (1991).
[55] K. Harafuji, A. Misaka, K. Kawakita, N. Nomura, H. Hamaguchi, M. Kawamoto, J. Vac. Sci. Technol. B, **10**(1), 133-142 (1992).
[56] P. Hudek, I. Rangelow, Lithography and reactive ion etching, publisher University of Kassel, Germany, (1998).

*Corresponding author: vutova@ie.bas.bg; victoria@netbg.com